A novel approach to treat the Thiel-Behnke corneal dystrophy using 3D printed honeycomb-shaped Polymethylmethacrylate (PMMA)/Vancomycin (VAN) scaffolds

Songul Ulag[1,2], Ali Sahin[3], Mehmet Mucahit Guncu[4], Burak Aksu[5], Nazmi Ekren[1,6], Mustafa Sengor[1,7], Deepak M. Kalaskar*[8], Oguzhan Gunduz[1,7**]

[1]Center for Nanotechnology & Biomaterials Application and Research (NBUAM), Marmara University, Turkey

[2]Department of Metallurgical and Materials Engineering, Institute of Pure and Applied Sciences, Marmara University, Turkey

[3]Department of Biochemistry, Faculty of Medicine, Marmara University, Istanbul, Turkey

[4]Institute of Health Sciences, Department of Microbiology, Marmara University, 34854, Turkey

[5]Department of Medical Microbiology, Marmara University School of Medicine, Istanbul, Turkey

[6]Department of Electric and Electronics Engineering, Faculty of Technology, Marmara University, Turkey

[7]Department of Metallurgical and Materials Engineering, Faculty of Technology, Marmara University, Turkey

[8]UCL Division of Surgery and Interventional Science, Royal Free Hospital Campus, University College London, Rowland Hill Street, NW3 2PF, United Kingdom

*d.kalaskar@ucl.ac.uk, **ucemogu@ucl.ac.uk

Abstract

Thiel-Behnke corneal dystrophy, or honeycomb corneal dystrophy, is an autosomal dominant corneal disorder. Tissue engineering can be a novel approach to regenerate this dystrophy. In this study, the honeycomb geometry of the dystrophy was mimicked with a 3D printing technology, and 40% PMMA, 40% PMMA/(0.1, 0.5, 2, and 10)% VAN scaffolds were fabricated with honeycomb geometry. As a result of the biocompatibility test with mesenchymal stem cells (MSCs), it can be said that cells on the scaffolds showed high viability and proliferation for all incubation periods. According to the antibacterial activity results, the 40% PMMA/10% VAN showed antibacterial activity against *S.aureous*. Mechanical results reported that with the addition of VAN into the 40% PMMA, the tensile strength value increased up to 2% VAN amount. The swelling behaviours of the scaffolds were examined *in vitro* and found that the swelling rate increased with a high VAN amount. The release of VAN from the scaffolds showed sustained release behaviour, and it took 13 days to be released entirely from the scaffolds.

Keywords: Corneal dystrophy; honeycomb; Thiel-Behnke; polymethylmethacrylate; vancomycin; 3D printing.

1.Introduction

The term corneal dystrophy includes a heterogeneous group of genetically determined non-inflammatory corneal diseases. Corneal dystrophies can be divided into three groups according to the single or dominant anatomical location of the abnormalities. Some primarily affect the corneal epithelium and its basement membrane or Bowman's layer and superficial corneal stroma, stromal corneal dystrophies or Descemet's membrane and corneal endothelium (posterior corneal dystrophies). Most corneal dystrophies have no systematic manifestations and are manifested by variable-shaped corneal opacities in a clear or cloudy cornea and affect visual acuity to varying degrees [1]. Thiel-Behnke corneal dystrophy (TBCD), or honeycomb corneal dystrophy, is an autosomal dominant corneal disorder, which has been described by Kuchle et al. as corneal dystrophy of Bowman's layer and superficial stroma type II (CDB II). Characteristic bilateral, honeycomb-like, subepithelial corneal recurrent erosive opacities are seen in patients between 10 and 20 years of age [2]. TBCD is an autosomal dominant hereditary disease that affects the whole cornea except the 1–2 mm peripheral part of the cornea. It occurs with rare recurrent erosions in infancy and is associated with diffuse-cloudy opacities that spread and become honeycomb-like over time [3]. Patients experience painful, recurrent, bilateral erosions that begin in early childhood. Then, progressive scar and eventually visual impairment are seen. TBCD is associated with severe vision loss requiring penetrating keratoplasty (PKP). PKP is the surgical removal of a damaged portion of the cornea followed by the implantation of healthy tissue from the donor cornea [4].

The slit-lamp examination shows honeycomb-shaped opacities confined to the Bowman layer and the superficial stroma area. Histopathologically, light microscopy reveals the marked irregularity of the epithelial thickness, the focal absence of the basement membrane of the epithelium, and the absence of the Bowman's layer. Electron microscopy findings include the partial lack of epithelial basement membrane and hemidesmosomal complex, absence of

Bowman's layer, and accumulation of "curly" collagen fibers between epithelium and superficial stroma [5]. TBCD-induced epithelial erosions can be treated first with topical antibiotics and artificial tears. Dystrophy recurs after simple debridement. Older patients may require lamellar or penetrating keratoplasty. However, relapses may occur one year after the postoperative period. Phototherapeutic keratectomy (PTK) is currently the first preferred treatment option. Thus, corneal transplantation can be delayed or even prevented [3]. PTK is an excimer laser-based surgical process performed by corneal surgeons to treat anterior corneal stromal pathologies. It helps by cutting the corneal stroma, improving corneal clarity and smoothing the surface [6].

Tissue engineering can be a novel approach to regenerate this dystrophy. In this study, the honeycomb geometry of the dystrophy was mimicked with a 3D printing process. Recently, with the rapid development of 3D printing technology, the design of complex three-dimensional spatial structures has become easier, and the preparation of porous composite materials with 3D printing technology has become appropriate [7]. PMMA was used as a matrix polymer, and it is generally used in additive surgery to treat both laser-assisted in situ keratomileusis and post-keratoconus corneal ectasia [8]. In addition, PMMA surrounds the cornea tissue and provides host tissue integration [9]. VAN was selected for initial investigation as a drug to treat the defected regions. Topical use of vancomycin is effective against almost all clinical strains of Gram-positive bacteria and significantly reduces the incidence of KPro-associated infectious endophthalmitis [10].

2.Materials and Method

2.1.Materials

Polymethyl methacrylate (MW = 12×10^4 g/mol) was supplied from Sigma Aldrich, USA. Dimethylformamide (DMF) and Tetrahydrofuran (THF) were taken from Merck KGaA, Germany. Vancomycin hydrochloride was obtained by Sigma Aldrich, USA.

2.2. Designing the 3D honeycomb model and G-code conversion

The 20x20x0.3 mm^3 3D scaffold model was designed with the Solidworks program, and this model was converted to the G-code with Simplify software. The Simplify program is the interface program of the 3D printer, and all settings are made here. Firstly, the fast honeycomb option was chosen and transformed the model into a honeycomb shape. 70% infill percentage was used to give pores to the model. The modified extrusion 3D printer (Ultimaker2+, Netherlands) was used to build the model in which the device has a heated build substrate and X-Y control head. The process parameters were adjusted to the properties of the solutions. The digital syringe pump connected to the 3D printer was utilized to feed the solutions. The 40% PMMA scaffold parameters were 0.3 mm nozzle diameter, 70% infill rate, and 0.3% extrusion multiplier. Only extrusion multiplier ratios was changed with VAN addition which were 0.3, 0.4, 0.4, 0.5 for 40% PMMA, 40% PMMA/0.1% VAN, 40% PMMA/0.5% VAN, 40% PMMA/2% VAN, and 40% PMMA/10% VAN, respectively. The prepared PMMA and PMMA/VAN solutions were transferred to a 10 mL luer lock syringe and put onto the syringe chamber of the device. First of all, the coordinates of the syringe were arranged and then the glass slide was put on the platform of the printer. After the optimization of the parameters, PMMA and PMMA/VAN scaffolds were printed. The 3D-printed scaffolds were carefully taken from the glass slide after complete drying.

2.3.Preparation of the PMMA and PMMA/VAN solutions

Firstly, 40wt.% PMMA solution was dissolved in 20 mL DCM:THF (50:50) at room temperature and dissolved at 300 rpm for 3 hours using a magnetic stirrer. Then, 0.1, 0.5, 2, and 10 wt.% VAN was added separately into the 40wt.% PMMA matrix to obtain VAN loaded blends and observe the VAN effect on the properties of the 40% PMMA matrix.

2.4. Characterization of the 3D-printed honeycomb-shaped PMMA/VAN scaffolds

2.4.1. Morphological analysis by SEM

A scanning electron microscope (SEM, MA-EVO10, ZEISS) was utilized to examine the morphological properties of the fabricated scaffolds.

2.4.2. Physicochemical properties of the honeycomb scaffolds

To observe the physicochemical properties of the 3D-printed scaffolds, fourier transform infrared spectroscopy (FT-IR, JASCO-4000) was used, which has 4000-400 cm^{-1} scanning range.

2.4.3. Thermal behaviours of the scaffolds

The thermal properties of the scaffolds were determined using a differential scanning calorimetry (DSC, DSC-6O Plus) machine. The heating rate of the process was 10°C/min, and the scanning temperature range was arranged from 25° C to 300° C.

2.4.4. Uniaxial tensile testing for mechanical characterizations

To determine the mechanical properties of the scaffolds, a tensile test was performed using the Shimadzu EZ-LX device with a force of 0.1 N, and 5 mm/min test speed was used during the test. Three scaffolds were used for all concentrations, and they were put directly between the jaws in the device.

2.4.5. *In vitro* swelling behaviours of the scaffolds

To observe the swelling capacities of the scaffolds, the swelling test was performed. In this test, scaffolds were put into PBS (pH=7.4) and shook on the thermal shaker at 37 °C with 250 rpm. The swelling test was performed for a week, and during the test, the same PBS was used. To calculate the swelling ratio of the scaffolds, Equation 2.1 [11] was used, which was given below.

$$S_R = \frac{W_S - W_D}{W_D} . 100 \qquad (2.1.)$$

W_S and W_D corresponded the swollen and dry weight values, respectively.

2.4.6. Investigation of the antimicrobial activities of the scaffolds

The bacterias were inoculated on Columbia Agar (Biomerieux, France) medium with 5% sheep blood the day before and left to incubate at 35-37 °C for 24 hours. One day later, the colony on the agar was removed, and a 0.5 McFarland turbidity cell suspension (1-5 * 10^8 cfu/mL) was prepared in the Müller Hinton Liquid medium (MHB) (Merck, Germany) in the cell densitometer device (Merck, Germany). Later, bacteria were spread on the medium of 90 mm Müller Hinton Agar (Merck, Germany) with a spreader device. The discs of the samples previously sterilized under ultraviolet light were placed on the medium. For *E. coli* ATCC 25922 and *S. aureus* ATCC 29213, the disk containing 10µg Imipenem and 30µg Cefoxitin was placed as the control disc, respectively. All samples were also placed in bacteria-free MHB for contamination analysis. Later, the media were incubated at 35-37 °C for 24 hours. The growth inhibition diameter around the disc after incubation was determined in mm.

2.4.7. Biocompatibility assessment

To observe the biocompatibility properties of the fabricated scaffolds, human adipose-derived mesenchymal stem cells was used as a cell line, which was obtained from American Type Culture Collection (ATCC, ATCC-PCS-500-011). To prepare the cells for the MTT assay, cells were incubated with Dulbecco's Modified Eagles Medium (DMEM) supplemented with 1% penicillin-streptomycin (Invitrogen) and 10% fetal bovine serum (FBS, Invitrogen). Firstly, scaffolds were sterilized with ultraviolet (UV) overnight in 24 well plates to prepare the samples for the MTT assay. First of all, all scaffolds were cultured in DMEM at 37° C, 5% CO_2 for 30 minutes. After half an hour, scaffolds were collected, and the rest medium was removed with a micropipette. In MTT protocol, scaffolds with 1x10^3 hASCs (cells/well) were cultured together at 37 °C, 5% CO_2 for 1, 4, and 7 days. To observe the cytotoxic properties of the scaffolds, 10 µg/mL MTT was used, and the absorbance measurement was carried out at 560 nm. All measurements were repeated with three samples, and their mean values were used. In the fixation procedure, the growth medium was removed from the plate and scaffolds were fixed

with 4% glutaraldehyde to examine the cellular structure on the scaffolds. Then, they were dehydrated with dilute ethanol. After the scaffolds had dried, they were mounted with Au for 60 s and examined under SEM at 10 kV.

2.4.8. *In vitro* release studies

The release behaviour of Van from PMMA scaffolds was carried out with PBS (pH: 7.4) at a thermal shaker (BIOSAN TS-100C). The first step of the drug release test is to determine the linear calibration curve of the VAN at 260-300 nm wavelength range using five different (2, 4, 6, 8, and 10 µg/ml) drug concentrations. The second step in the drug release test is observing the release behaviours of VAN at different time intervals. Firstly, 5 mg VAN-loaded PMMA scaffolds were weighed and put into eppendorf tubes with 1 ml PBS (pH=7.4). Scaffolds were kept into PBS for 15 min, 30 min, 1, 2, 3, 5, 24, 48, 96, 120, 144, 168, 192, 216, 240, 264, 298, 320, and 344 hours. During the test, fresh PBS was used after each measurement. UV-Vis Spectrophotometer (Shimadzu, Japan) was used to detect the absorbance values of the drug at 285 nm wavelength.

2.4.9. Statistical analyses

All experiments were performed on triplicate datasets (N = 3). The ANOVA software was used to determine the statistical analysis. The level of significance was taken $p < 0.05$ and labelled with "*". The mark "**" represented the $p<0.01$. The drug release test was given as the mean ± standard error of the mean.

3. Results and Discussions

3.1. Morphological properties of the honeycomb patterns

The SEM images of the honeycomb-shaped scaffolds with honeycomb pores were given in Figure 1. The images showed a regular honeycomb arrangement of pores for all concentrations. These suitable honeycomb structures were fabricated by adjusting 3D process parameters. It can be said that different concentrations of VAN each have their optimum flow rate to fabricate

the well-defined honeycomb patterns. The high magnification images also showed that the honeycomb units were stacked neatly and bonded well together [12]. Some studies reported that scaffolds with honeycomb patterns could better mimic the cell morphology [13]. Thus, honeycomb patterns fabricated in this study can allow more cells to adhesion to the pattern and enhance proliferation. The full-thickness tissue constructs composed of cell-planted ECM can be successfully implanted in a clinical reconstructive setting only when vascular networks are provided. Vascular networks distribute oxygen and nutrients within the matrix. In thin-thickness designed tissues such as skin, nutrient uptake and waste removal occur by diffusion until vascularization is achieved [14]. The thickness of the scaffolds was measured with SEM in this study. It was found that these values were almost the same for all scaffolds and ranged between 0.1 mm to 0.15 mm. The mean pore size values of the scaffolds were calculated using SPSS software, and their distributions were given in Figure 1. The mean pore size value of the 40% PMMA was found to be 672.15±69.76 µm. This value increased with VAN addition and the highest pore size value belonged to the 40% PMMA/10% VAN scaffold.

3.2. FTIR analysis of the VAN and PMMA/VAN scaffolds

Figure 2 A (a), the FTIR spectrum of the Vancomycin hydrochloride showed characteristic peaks in the band of 3257.18 cm^{-1} of hydroxyl stretch, 1644.98 cm^{-1} of C=O stretch, 1585.20 cm^{-1} of C=C and 1226.50 cm^{-1} of phenolic hydroxyl groups [15]. The main peaks of the pure PMMA spectrum are: C-H stretching (2950.55 cm^{-1}) and bending (1481.06–1386.57 cm^{-1}) modes; C=O stretch mode (1722.12 cm^{-1}); and three bands in the 1386.57–1143.58 cm^{-1} region of the spectrum assigned to ester group stretch vibrations or skeletal vibrations (1189.86 and 1143.58 cm^{-1}) due to combined CO and antisymmetric C-C-O stress (1240 cm^{-1}) and C-H deformations. The band at 840.81 cm^{-1} is assigned to the methylene rocking mode [16]. There is no peak in the 600-650 range in the PMMA FTIR spectrum. The peaks observed in the 600-650 range in the PMMA/VAN scaffolds were occurred by the VAN effect. However, other

peaks of the PMMA/VAN scaffolds is similar to that of PMMA, meaning that the VAN was successfully loaded into PMMA [17].

3.3. Thermal behaviours of the scaffolds

Figure 2B demonstrated the DSC curves of the pure powder VAN and PMMA, PMMA/VAN scaffolds. The pure vancomycin DSC graph showed only a broad endotherm at 125.4° C due to drug decomposition. This endothermic peak is due to the decomposition of the drug [18]. It can be said that the peak observed at 48.23°C in the DSC curve of the 40% PMMA scaffold is due to a slight weight loss, probably related to the evaporation of the residual solvent (DCM: THF) [19]. The same behaviour was also observed in the VAN-loaded scaffolds with slight shifts to the right. The maximum temperature shift (from 48.23 °C to 64.07 °C.) was observed for 40% PMMA/10% VAN scaffold. The similarity of DSC curves of all scaffolds indicated no incompatibility between VAN and PMMA [20].

3.4. Tensile testing results of the scaffolds

It is essential to examine the mechanical behaviours of the corneal scaffolds under the influence of force. The tensile testing results of the 3D-printed scaffolds are given in Table 1. When the tensile results were examined, the tensile strength of 40% PMMA scaffold was found 0.33±0.31 MPa and the strain value was found 0.80±0.22 %. The tensile strength value of the 40% PMMA/0.1% VAN scaffold reached 2.22±1.82 MPa, and the strain value also increased to 2.75±1.13 %. Adding 0.5% VAN into the 40% PMMA further increased the tensile strength value to 2.82±1.73 MPa. In addition, the strain value reached 3.05±1.35 %. On the other hand, adding 2% VAN into the 40% PMMA reduced the tensile strength to 0.68±0.31 MPa and the strain value to 1.28±0.13 %. However, these values are still higher than the strength and strain values of the 40% PMMA scaffold. The addition of 10% VAN into the 40% PMMA caused to increase in the tensile strength value again (0.905±0.3 MPa), but the strain value continued to decrease (0.202±0.11 %). It is known that the addition of low molecular weight drug can cause

the plasticizing affect on the structures [21]. In this study, by the addition of 0.1, 0.5, and 2 % VAN into the 40% PMMA, the strain value of the 40% PMMA increased. This proved the plasticizing effect of the low molecular weight VAN. On the other hand, with the 10% VAN addition, the strain value decreased distinctly and has the lowest value among all scaffolds. It can be said that the plasticity of the scaffolds decreased with the increase of the strength value again. Li et al. tested the high dose of vancomycin and gentamicin into the bone cement and found that a high dose of VAN decreased the mechanical strength from 93.86±2.13 MPa to 70.52±1.43 MPa with the VAN ratio from 2.5% to 10% [22]. Another study performed by Lee et al. found that the compressive strength of vancomycin-loaded bone cement declined to 38%, with the addition of VAN increased from 1.25% to 10% [23].

3.5. Swelling behaviours of the scaffolds

The ability of scaffolds to absorb water or swell is an important parameter that ensures the absorption and transfer of body fluids, wound exudates, and cell nutrients within the scaffold. Under physiological conditions, the swelling must be controlled to prevent rapid degradation and mechanical weakening of scaffolds [24]. The swelling results of the scaffolds are given in Figure 3. When the one-day swelling results were examined, the highest swelling rate was observed for the 40% PMMA/10% VAN added, and it was observed that the swelling percentage increased as the VAN rate increased. The lowest swelling rate was 40% PMMA. A high increase was observed for all scaffolds on the second day, and the highest swelling rate was observed for the 40% PMMA/10% VAN scaffold. When the three-day swelling results were examined, the swelling rate started to decrease for 40% PMMA and 40% PMMA/0.1% VAN scaffolds. On day 5, swelling rates decreased for all the scaffolds, and on the 6th day, the decrease in swelling rates continued.

3.6. Antibacterial activities of the scaffolds

Different volumes and concentrations of vancomycin should be tested to confirm antibacterial activity [25]. The antimicrobial activities of the scaffolds are given in Table 2 and Figure 4. The results showed that only 40% PMMA/10% VAN scaffold had antimicrobial activity against the *S.aureous* with a 12 mm inhibition zone, but it didn't show the antimicrobial activity against the *E. coli*. As previously noted, the antimicrobial results demonstrated that the incorporation of antimicrobial drug into scaffolds did not compromise its natural antibacterial activity [26]. In addition, the reason for the lack of antibacterial effect of 40% PMMA/10% VAN scaffold against *E.coli* is the resistance of the gram-negative bacteria to vancomycin, which cannot significantly penetrate the outer membrane [27].

3.7. Biocompatibility properties of the scaffolds

The cell proliferation ability was examined by the MTT assay shown in Figure 5. After 1 day of incubation, all scaffolds showed high viability even at the early stage. The maximum viability value observed for 40% PMMA/2% VAN scaffold is 128.1±16.52 %. The 40% PMMA had the minimum viability value (99.3±8.03) compared to the VAN-added scaffolds. On day 3, the viability values of all scaffolds increased, and all scaffolds had a higher viability percentage compared to the 2D (MSC). The maximum viability value (133.4±9.76) was observed for 40% PMMA scaffold, and the minimum viability value (110.5±1.36) was observed for 40% PMMA/10% VAN scaffold. As the incubation proceeded to the 3rd day, a significant increase in the cell proliferation on scaffolds was observed. When the viability values of the VAN added scaffolds were compared for the three days incubation, the highest viability value was observed in the 40% PMMA/0.1% VAN scaffold. The lowest viability value belonged to the 40% PMMA/10% VAN scaffold. When the viability values were examined after 7 days of incubation, a decrease was observed in the viability values for all scaffolds. However, the viability values for all scaffolds are higher than the control group (100%). This showed that the biocompatibility properties of the scaffolds were relatively high. Moreover, VAN inhibits

bacterial cell wall synthesis by binding to the terminal D-Ala-D-Ala dipeptide of peptido-glycan units. This can explain why vancomycin has no cytotoxic effect on MSCs [28].

Figure 6 demonstrated the fluorescence images of the honeycomb-shaped scaffolds after 7 days of incubation. In Figure 6a, it was seen that the cells were spread over the entire surface of the 40% PMMA scaffold and were dense. Figure 6b showed the cell distribution on the 40% PMMA/0.1% VAN scaffold. The images showed fewer cells on this scaffold, and they were not distributed over the scaffold. The fluorescence images of the 40% PMMA/0.5% VAN are shown in Figure 6c. It was seen that the number of cells was higher than the 40% PMMA/0.1% VAN scaffold, but it was still not enough for cell proliferation. The number of cells was getting higher with the addition of 2% VAN into the 40% PMMA matrix (Figure 6d). It was seen that cells were spread all over the scaffold, and images also showed that cells proliferated sufficiently on the scaffold. Figure 6e represented the fluorescence images of the 40% PMMA/10% VAN scaffold and reported that the cells spread and proliferated effectively on the scaffold, but relatively less than the number of cells at 40% PMMA/2% VAN scaffold.

On the 7^{th} day of the culture, the morphologies and attachment of the MSCs on the 3D-printed scaffolds were investigated with SEM in Figure 7. Typical MSC morphologies were observed on the scaffolds. It was seen that cells attached to the surface of the scaffolds and spread on the entire scaffolds with their filopodias [21].

3.8. Drug release profiles of the VAN from the scaffolds

The release of VAN from the 3D-printed scaffolds was investigated in a PBS at the thermal shaker. The standard curve of the VAN was obtained from stock solutions (0.25, 0.5, 1, 1.5, and 2 μg/mL) and given in Figure 8a. Figure 8b shows the absorption graph of the VAN detected at 285 nm. Figure 8c represents the cumulative release of VAN from the different formulations. According to the graph, in the first 15 minutes, 400% PMMA/0.1% VAN scaffold had 0.11%, 40% PMMA/0.5% VAN scaffold had 8.35%, 40% PMMA/2% VAN scaffold had 5,34%, and

40% PMMA/10% VAN scaffold had 10.47% release percentages. The highest release percentage belonged to the 400% PMMA/10% VAN scaffold for 15 minutes. After 2 hours, 40% PMMA/10% VAN scaffold was the highest release amount with a release percentage of 25.92%. After 7200 minutes, VAN release from the scaffolds reached nearly 50% release percentages. VAN release from all scaffolds reached 100% cumulative release after 13 days of the incubation period. The release of the VAN from the scaffolds was prolonged and controlled, which indicated that these drug-loaded scaffolds could be used as a drug carrier for their slow release behaviour [29]. Long-term and controlled release of the drug is important clinically in terms of lower dosing frequency, maximum drug use that reduces the total dose, and the intensity of the local and systemic side effects of the drug [30].

Conclusions

In this research, VAN-loaded honeycomb-shaped scaffolds were successfully fabricated with a 3D printing process and evaluated for their potentials to regenerate the Thiel-Behnke corneal dystrophy. The SEM images showed the capability of 3D printing and materials to form 3D honeycomb-shaped scaffolds. The mechanical properties were determined with tensile testing, and results demonstrated that VAN addition increased the tensile strength value compared to the 40% PMMA scaffold. The drug release profile of VAN from the scaffolds showed sustained release up to 13 days. *In vitro* cytotoxicity assay of the scaffolds with the MSCs verified their biocompatibility. The cell densities and morphologies of the scaffolds after 7 days of culture showed that cells were highly attached and proliferated on the scaffolds. The antimicrobial activity results showed that only 40% PMMA/10% VAN scaffold showed antibacterial activity against the *S.aureous*.

Acknowledgements

The authors thank Marmara University Scientific Research Committee (FDK-2020-10117) for their financial support.

Data availability

The raw data will be made available upon request.

References

1. G. K. Klintworth. Corneal dystrophies. Orphanet Journal of Rare Diseases, 7 (2009), pp. 1-38.
2. A. Kobayashi, S. Ijiri, T. Ohta, K. Sugiyama. Disappearance of Honeycomb Opacity of Thiel-Behnke Corneal Dystrophy After Thygeson Superficial Punctate Keratitis. Cornea, 24 (2005), pp. 1029-1030.
3. W. Lisch, A. Janecke, B. Seitz. Corneal Dystrophy, Thiel-Behnke. In: Lang F. (eds) Encyclopedia of Molecular Mechanisms of Disease. Springer, Berlin, Heidelberg, 2009, pp. 440.
4. M. A. Abu-Ameerh, M. D. Al-Bdour, B. Moh'd Al-Rawashdeh, K. Al-Haidar, S. Khraisat, A. Abed, S. A. AlRyalat, Y. A. H. Abu Gharbieh, F. Al-Haidar. Outcome of Penetrating Keratoplasty (PKP) and Redo PKP among Jordanian Population. Research in Health Science, 4 (2019), p.273.
5. L. S. Sullivan, X. Zhao, S. J. Bowne, X. Xu, S. P. Daiger, S. B. Yee, R. W. Yee. Exclusion of the human collagen type XVII (COL17A1) gene as the cause of Thiel-Behnke corneal dystrophy (CDB2) on chromosome 10q23-q25. Current Eye Research, 27 (2003), pp. 223–226.
6. R. Nagpal, P. K. Maharana, P. Roop, S. Murthy, C. J. Rapuano, J. S. Titiyal, R. B. Vajpayee, N. Sharma. Phototherapeutic Keratectomy. Surv Ophthalmol., 65 (2020), 65, pp. 79-108.
7. H. Hong, M. Hu, L. Dai. Dynamic Mechanical Behavior of Hierarchical Resin Honeycomb by 3D Printing. Polymers, 13 (2021), pp. 1-14.

8. J. Merayo-Lloves, T. Blanco-Mezquita, L. Ibares-Frías, L. Fabiani, A. Alvarez-Barcia, C. Martinez-García. Induction of controlled wound healing with PMMA segments in the deep stroma in corneas of hens. Eur J Ophthalmol, 20 (2010), pp.62-70.
9. A. K. Riau, D. Mondal, G. H. F. Yam, M. Setiawan, B. Liedberg, S. S. Venkatraman, J. S. Mehta. Surface Modification of PMMA to Improve Adhesion to Corneal Substitutes in a Synthetic Core−Skirt Keratoprosthesis. ACS Appl. Mater. Interfaces, 7 (2015), pp. 21690–21702.
10. A. K. Riau, D. Mondal, T. T. Aung, E. Murugan, L. Chen, N. C. Lwin, L. Zhou, R. W. Beuerman, B. Liedberg, S. S. Venkatraman, J. S. Mehta. Collagen-Based Artificial Corneal Scaffold with Anti-Infective Capability for Prevention of Perioperative Bacterial Infections. ACS Biomater. Sci. Eng. 1 (2015), pp. 1324−1334.
11. E. A. Kamoun, X. Chen, M. S. M. Eldin, ER. S. Kenawy. Crosslinked poly(vinyl alcohol) hydrogels for wound dressing applications: A review of remarkably blended polymers. Arabian Journal of Chemistry, 8 (2015), pp. 1-14.
12. T. Yao, H. Chen, P. Samal, S. Giselbrecht, M. B. Baker, L. Moroni. Self-assembly of electrospun nanofibers into gradient honeycomb structures. Materials & Design, 168, 2019, 107614.
13. M. A. Birch, M. Tanaka, G. Kirmizidis, S. Yamamoto, and M. Shimomura, "Microporous "Honeycomb" films support enhanced bone formation in vitro," Tissue Engineering Part A, vol. 19, no. 17-18, pp. 2087-2096.
14. V. J. Hondt, M. Den. Tissue engineering and surgery: from translational studies to human trials. Innovative Surgical Sciences, 2 (2017), pp. 189-202.
15. H. B. Mohamed, S. M. El-Shanawany, M. A. Hamad, M. Elsabahy. Niosomes: A Strategy toward Prevention of Clinically Signifcant Drug Incompatibilities. Scientific Reports, 7 (2017), pp. 6340.

16. S. Sain, D. Ray, A. Mukhopadhyay, S. Sengupta, T. Kar, C. J. Ennis, K. S. Pattanathu, M. Rahman. Synthesis and Characterization of PMMA-Cellulose Nanocomposites by In Situ Polymerization Technique. Journal of Applied Polymer Science, 126 (2012), pp. E127–E134.
17. B. Gumus, T. Acar, T. Atabey, S. Derman, F. Sahin, T. Arasoglu. The battle against biofilm infections: juglone loaded nanoparticles as an anticandidal agent. Journal of Biotechnology, 316 (2020), pp. 17–26.
18. A. F. C. Resende, A. F. Pereira, T. P. Moreira, P. S. O. Patrício, S. L. Fialho, G. M. F. Cunha, A. Silva-Cunha, J. T. Magalhães, G. R. Silva. PLGA Implants containing vancomycin and dexamethasone: development, characterization and bactericidal effects. Pharmazie, 71 (2016), 439-446.
19. R. C. Sanfelice, L. A. Mercante, A. Pavinatto, N. B. Tomazio, C. R. Mendonc¸ S. J. L. Ribeiro, L. H. C. Mattoso, D. S. Correa. Hybrid composite material based on polythiophene derivative nanofibers modified with gold nanoparticles for optoelectronics applications. J Mater Sci., 52 (2017), pp. 1919–1929.
20. N. S. Maram, M. Jelvehgari, L. Vaccaro, D. Lanari, L. Mafakher, A. Z. Ahmady. Preparation of Vancomycin Hydrochloride Nanoparticles and Survey of the Factors Influence their Properties. Orient. J. Chem., 33 (2017), pp. 575-583.
21. M. Zhang, Z. Li, L. Liu, Z. Sun, W. Ma, Z. Zhang, R. Zhang, D. Sun. Preparation and Characterization of Vancomycin-Loaded Electrospun Rana chensinensis Skin Collagen/Poly(L-lactide) Nanofibers for Drug Delivery. Journal of Nanomaterials, 2016, pp. 9159364.
22. T. Li, L. Fu, J. Wang, Z. Shi. High dose of vancomycin plus gentamicin incorporated acrylic bone cement decreased the elution of vancomycin. Infection and Drug Resistance, 12 (2019), pp. 2191–2199.

23. SH. Lee, CL. Tai, SY. Chen, CH. Chang, YH. Chang, PH. Hsieh. Elution and Mechanical Strength of Vancomycin-Loaded Bone Cement: In Vitro Study of the Influence of Brand Combination. PLoS One, 11 (2016), pp. e0166545.
24. K. Aranci, M. Uzun, S. Su, S. Cesur, S. Ulag, A. Amin, M. M. Guncu, B. Aksu, S. Kolayli, C. B. Ustundag, J. C. Silva, D. Ficai, A. Ficai, O. Gunduz. 3D Propolis-Sodium Alginate Scaffolds: Influence on Structural Parameters, Release Mechanisms, Cell Cytotoxicity and Antibacterial Activity. Molecules, 25 (2020), 5082.
25. A. Eidmann, A. Ewald, S. P. Boelch, M. Rudert, B. M. Holzapfel, I. Stratos. In vitro evaluation of antibacterial efficacy of vancomycin-loaded suture tapes and cerclage wires. Journal of Materials Science: Materials in Medicine, 42 (2021), pp. 32:42.
26. H. A. Fathia, A. Abdelkadera, M. S. AbdelKarim, A. A. Abdelaziz, M. A. El-Mokhtar, A. Allame, G. Fetiha, M. El Badrya, M. Elsabahy. Electrospun vancomycin-loaded nanofibers for management of methicillin-resistant Staphylococcus aureus-induced skin infections. International Journal of Pharmaceutics, 586 (2020), pp. 119620.
27. A. Zhou, T. M. Kang, J. Yuan, C. Beppler, C. Nguyen, Z. Mao, M.Q. Nguyen, P. Yeh, J. H. Miller. Synergistic Interactions of Vancomycin with Different Antibiotics against Escherichia coli: Trimethoprim and Nitrofurantoin Display Strong Synergies with Vancomycin against Wild-Type E. coli. Antimicrobial Agents and Chemotherapy, 59 (2015), pp. 276–281.
28. E. Booysen, H. SV. Gijsen, S. M. Deane, W. Ferris, L. M. T. Dicks. The Effect of Vancomycin on the Viability and Osteogenic Potentialof Bone-Derived Mesenchymal Stem Cells. Probiotics and Antimicrobial Proteins, 11 (2019), pp. 1009–1014.
29. S. Ulag, E. Ilhan, A. Sahin, B. K. Yilmaz, N. Ekren, O. Kilic, F. N. Oktar, O. Gunduz. 3D printed artificial cornea for corneal stromal transplantation. European Polymer Journal, 133 (2020), pp. 109744.

30. P. Mandhar, G. Joshi. Development of Sustained Release Drug Delivery System: A Review. Asian Pac. J. Health Sci., 2 (2015), 179-185.

Graphical abstract

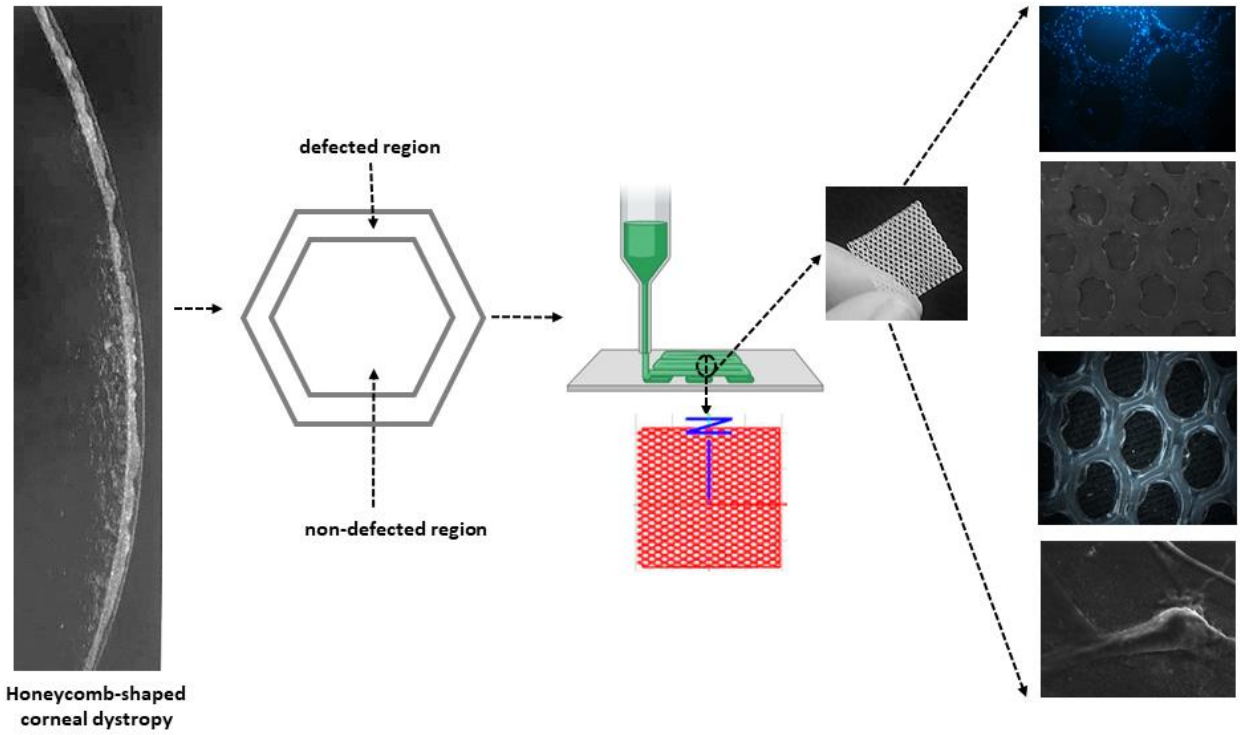

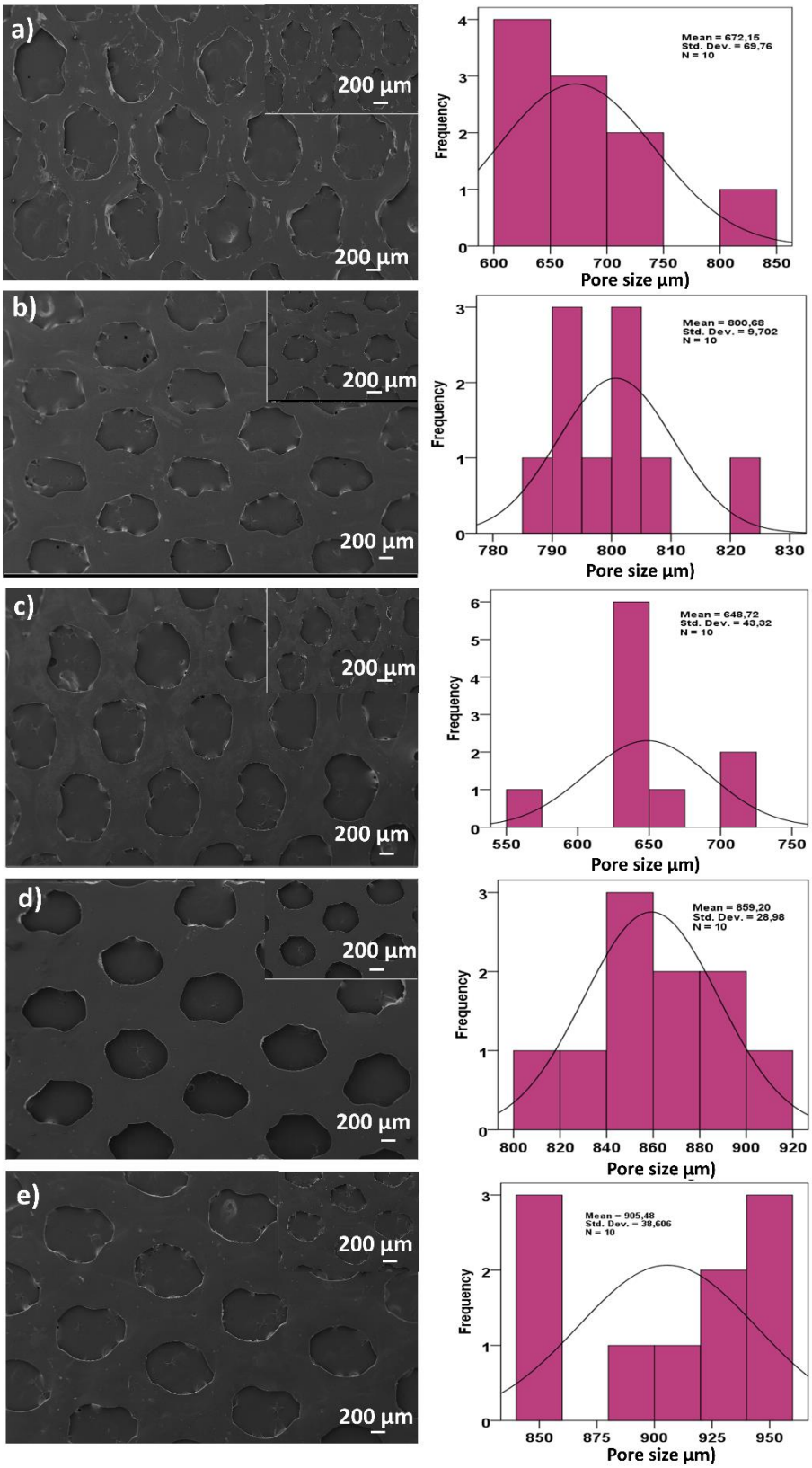

Figure 1. The SEM images of the 40% PMMA (a), 40% PMMA/0.1% VAN (b), 40% PMMA/0.5% VAN (c), 40% PMMA/2% VAN (d), 40% PMMA/10% VAN (e) with their pore size distributions.

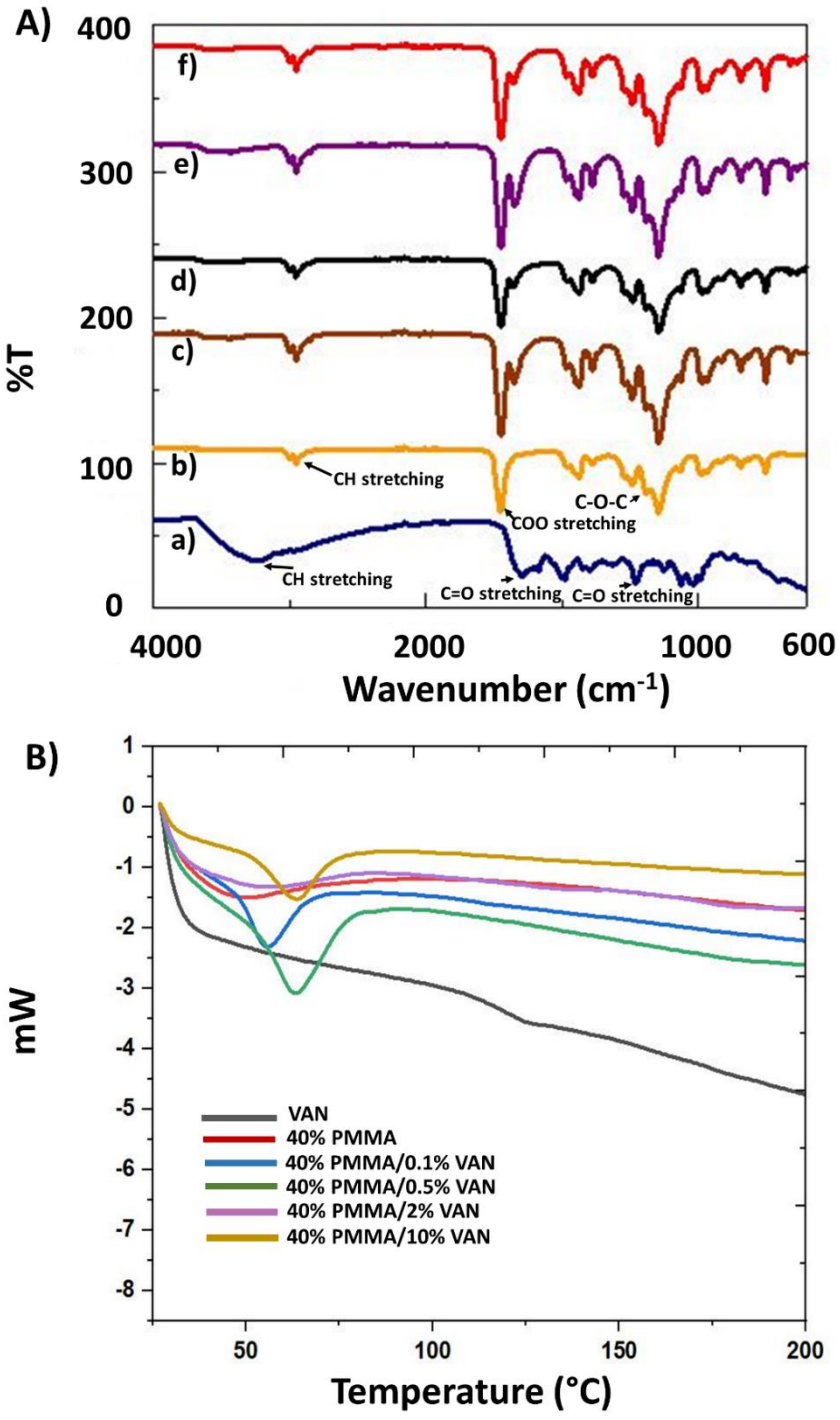

Figure 2. FTIR spectrums of the pristine Vancomycin (A, a), 40% PMMA (A, b), 40% PMMA/0.1% VAN (A, c), 40% PMMA/0.5% VAN (A, d), 40% PMMA/2% VAN (A, e), and 40% PMMA/10% VAN (A, f). The DSC curves of the pure VAN and PMMA/VAN scaffolds (B).

Table 1. The tensile test results of the 3D-printed scaffolds.

Scaffolds	Tensile strength (MPa)	Elongation at break (%)
40% PMMA	0.33±0.314	0.81±0.224
40% PMMA/0.1% VAN	2.22±1.82	2.75±1.13
40% PMMA/0.5% VAN	2.82±1.73	3.05±1.35
40% PMMA/2% VAN	0.68±0.31	1.28±0.13
40% PMMA/10% VAN	0.91±0.3	0.202±0.11

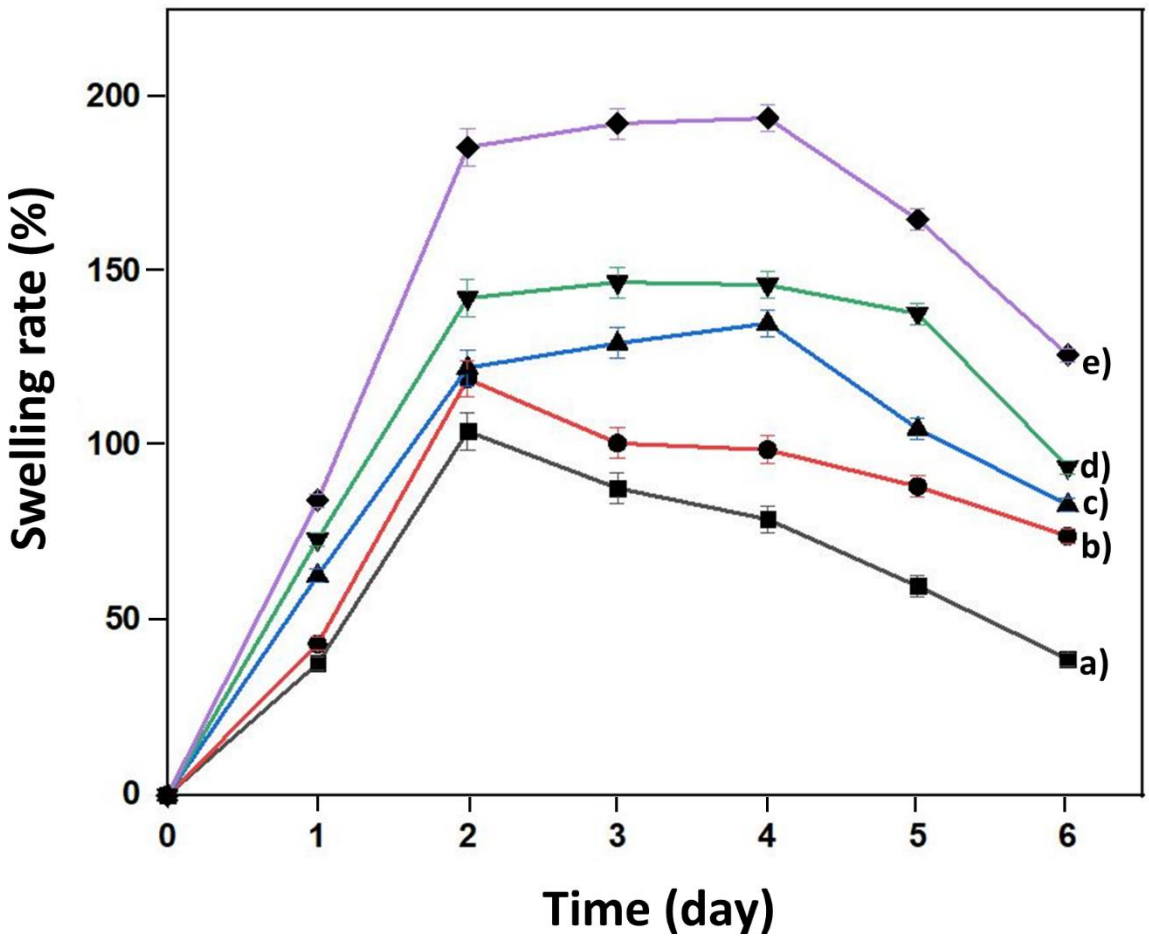

Figure 3. The swelling behaviours of the scaffolds in the liquid medium; 40% PMMA (a), 40% 5PMMA/0.1% VAN (b), 40% PMMA/0.5% VAN (c), 40% PMMA/2% VAN (d), and 40% PMMA/10% VAN (e).

Table 2. Antimicrobial activity results of the scaffolds against the *S.aureus* and *E. coli*.

Scaffolds	***S. aureus* ATCC 29212 (Inhibition zone, mm)**	***E. coli* ATCC 25922 (Inhibition zone, mm)**
40% PMMA/0.1% VAN	0	0
40% PMMA/0.5% VAN	0	0
40% PMMA/2% VAN	0	0
40% PMMA/10% VAN	12	0
Control	0	-
Cefoxitin (30 µg)*	30	-
Imipenem (10 µg)*	-	30

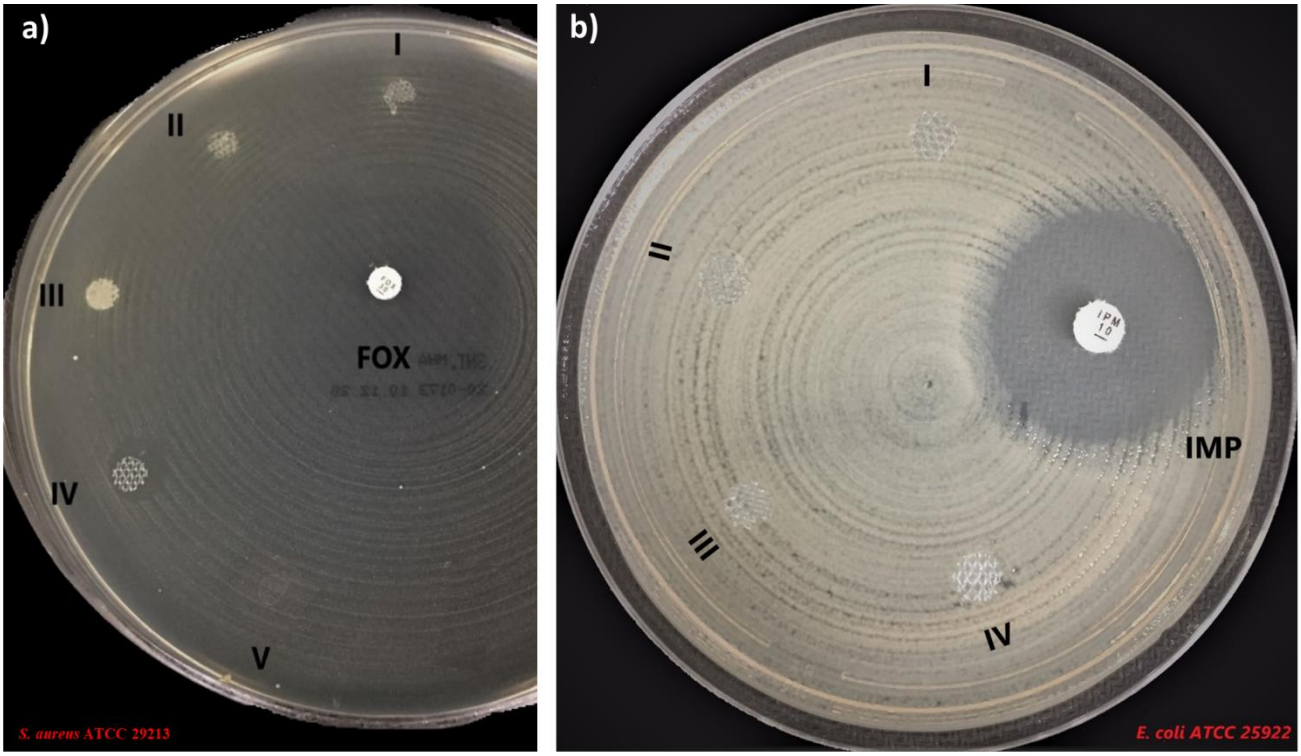

Figure 4. The antimicrobial activities of the scaffolds against the *S. aureus* (a), and *E. coli* (b).

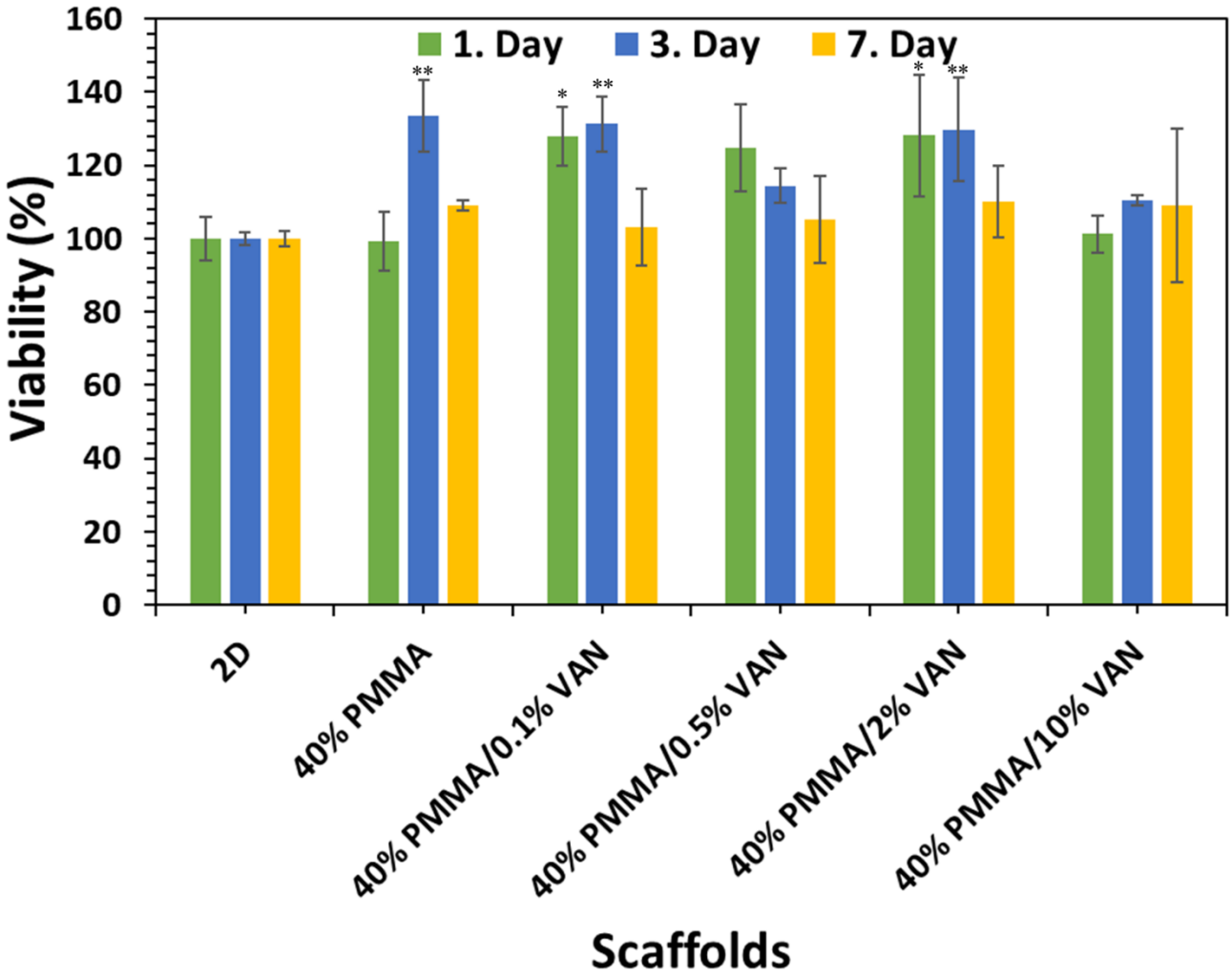

Figure 5. MTT graph of the scaffolds after 1, 3, and 7 days of incubation. The mark "*" represented the significant differences $p < 0.05$ and "**" $p < 0.01$.

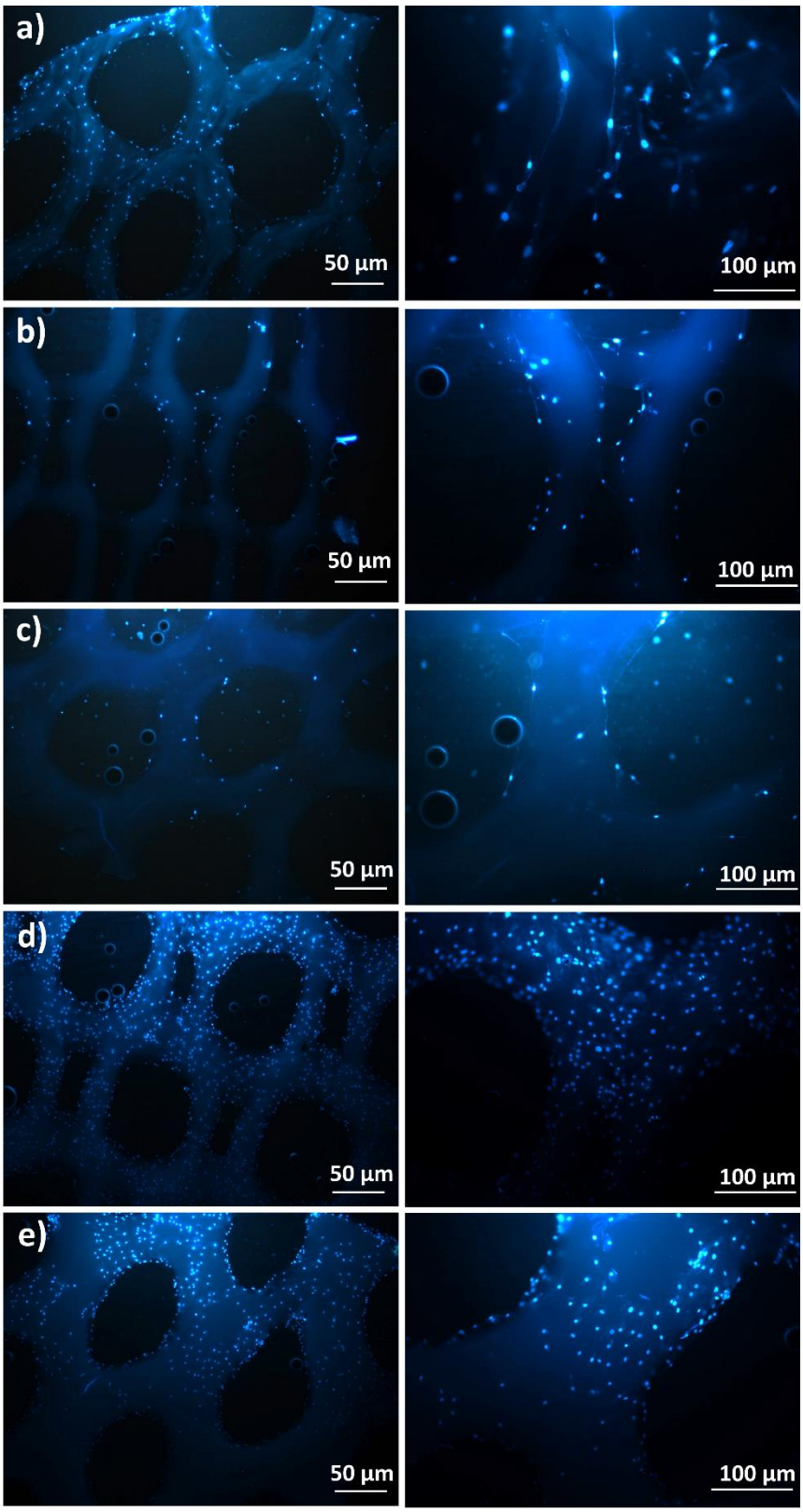

Figure 6. The DAPI stained MSCs on the 3D-printed 40% PMMA (a), 40% PMMA/0.1% VAN (b), 40% PMMA/0.5% VAN (c), 40% PMMA/2% VAN (d), and 40% PMMA/10% VAN (e) scaffolds after 7 days of culture period.

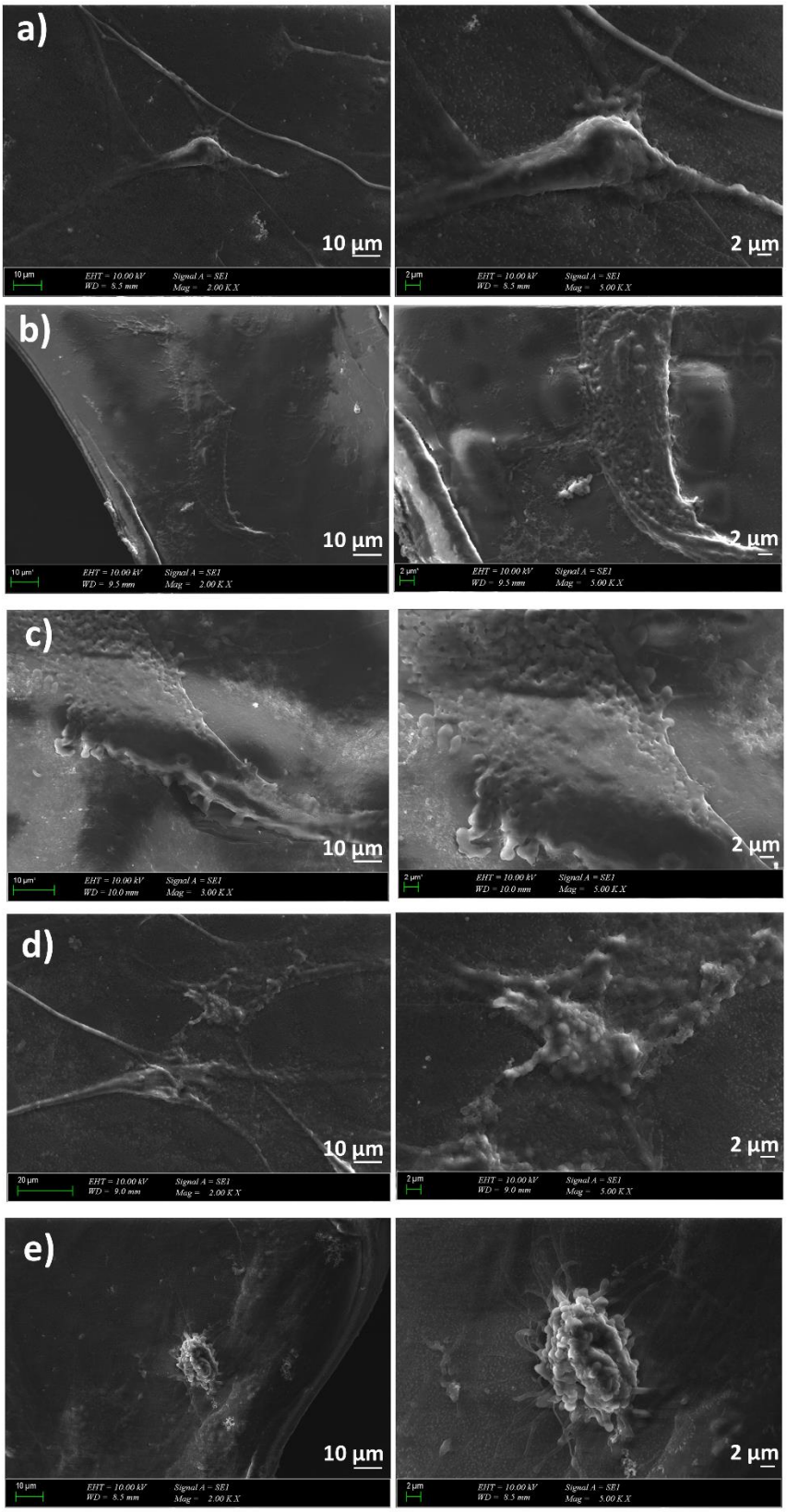

Figure 7. The morphologies of the MSCs on the scaffolds; 40% PMMA (a), 40% PMMA/0.1% VAN (b), 40% PMMA/0.5% VAN (c), 40% PMMA/2% VAN (d), and 40% PMMA/10% VAN (e) after 7 days of incubation.

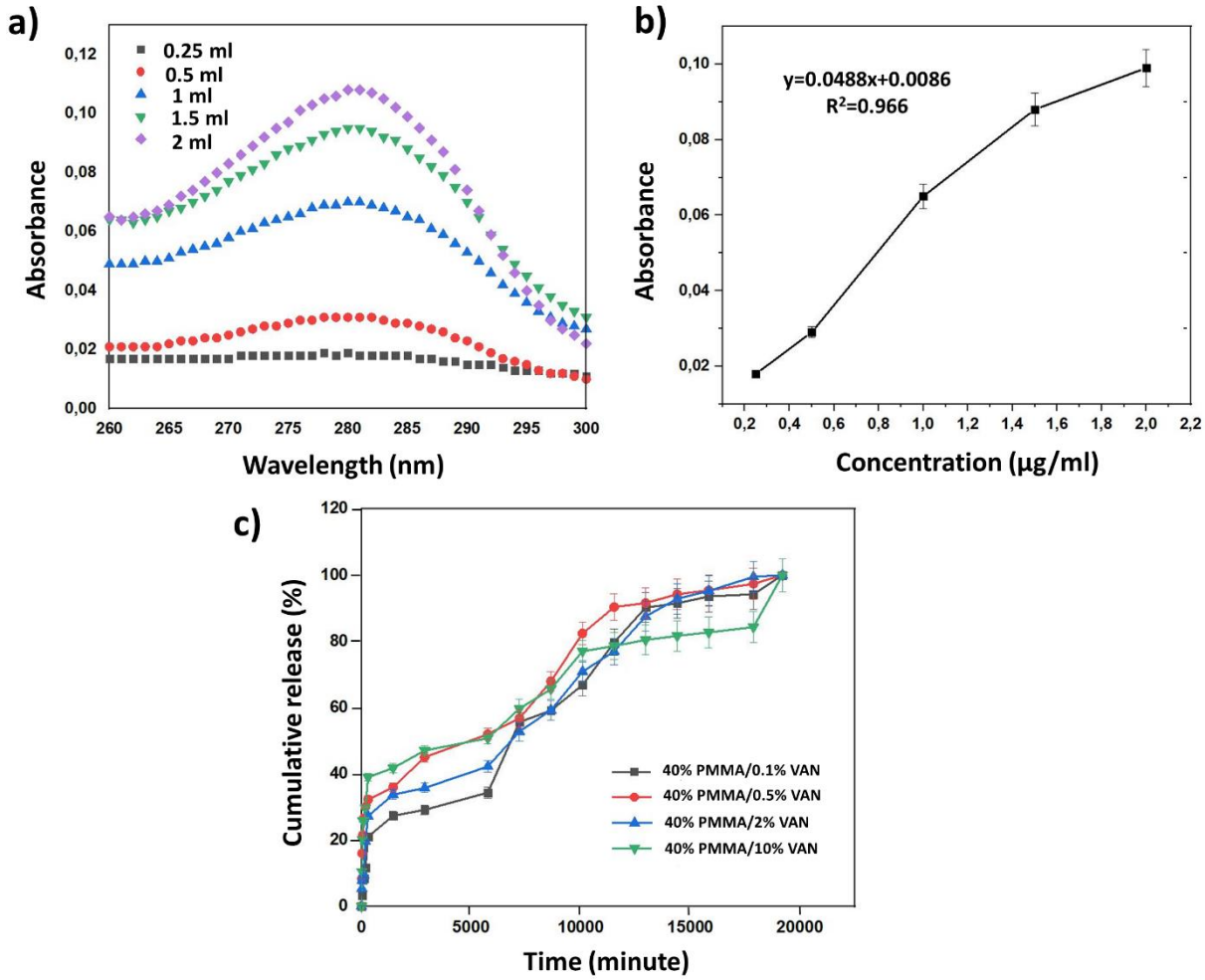

Figure 8. The standard curve of the VAN (a), absorbance graph obtained from the calibration curve (b), the release behaviour of the VAN from the 3D-printed scaffolds (c).